Mixed signals: interpreting mixing patterns of different soil bioturbation processes through luminescence and numerical modelling

Willem Marijn van der Meij[1], Svenja Riedesel[1,2], Tony Reimann[1]

[1] Institute of Geography, University of Cologne, Zülpicher Straße 45, 50674 Cologne, Germany

[2] Department of Physics, Technical University of Denmark, Frederiksborgvej 399, 4000 Roskilde, Denmark

Correspondence to: W. Marijn van der Meij (m.vandermeij@uni-koeln.de)

Abstract. Soil bioturbation plays a key role in soil functions such as carbon and nutrient cycling. Despite its importance, fundamental knowledge on how different organisms and processes impact the rates and patterns of soil mixing during bioturbation is lacking. However, this information is essential for understanding the effects of bioturbation in present-day soil functions and on long-term soil evolution.

Luminescence, a light-sensitive mineral property, serves as a valuable tracer for soil bioturbation. The luminescence signal resets (bleaches) when a soil particle is exposed to daylight at the soil surface and accumulates when the particle is buried in the soil, acting as a proxy for subsurface residence times. In this study, we compiled three luminescence-based datasets of soil mixing by different biota and compared them to numerical simulations of bioturbation using the soil-landscape evolution model ChronoLorica. The goal was to understand how different mixing processes affect depth profiles of luminescence-based metrics, such as the modal age, width of the age distributions and the fraction of bleached particles.

We focus on two main bioturbation processes: mounding (advective transport of soil material to the surface) and subsurface mixing (diffusive subsurface transport). Each process has a distinct effect on the luminescence metrics, which we summarized in a conceptual diagram to help with qualitative interpretation of luminescence-based depth profiles. A first attempt to derive quantitative information from luminescence datasets through model calibration showed promising results, but also highlighted gaps in data that must be addressed before accurate, quantitative estimates of bioturbation rates and processes are possible.

The new numerical formulations of bioturbation, which are provided in an accompanying modelling tool, provide new possibilities for calibration and more accurate simulation of the processes in soil function and soil evolution models.

Keywords: Bioturbation, luminescence, soil evolution, numerical modelling

1 Introduction

30 Bioturbation is a fundamental process of soil mixing by different biota that plays a key role in nutrient cycling, carbon sequestration, erosion, and in the distribution of contaminants and pollutants (Wilkinson et al., 2009; Briones, 2014; Creamer et al., 2022). Despite its pivotal role in regulating soil functions, there is still a deficiency in fundamentally understanding how different organisms impact the rates and directions of soil fluxes during bioturbation (Schiffers et al., 2011; Michel et al., 2022). These insights are essential for accurately modelling the effects of bioturbation on present-day soil functions and the

35 long-term evolution of soils (Creamer et al., 2022; Meng et al., 2022).

In this work, we focus on two types of soil bioturbation processes: mounding and subsurface mixing (Wilkinson et al., 2009). *Mounding* is the upward advective transport of soil material, which is deposited on the surface in mounds and later eroded and buried by newly mounded material (e.g., by gophers and termites; Gabet, 2000; Kristensen et al., 2015). *Subsurface mixing* is the diffusive up- and downward exchange of soil material throughout the entire soil profile at various depths (e.g., by endogeic

40 and anecic earthworms and galley-building ants; Richards, 2009; Halfen and Hasiotis, 2010; Taylor et al., 2019). Bioturbation is often an interplay of mounding and subsurface mixing, driven by environmental and climatic factors (Wilkinson et al., 2009; Kraus et al., 2022), which leads to mixed bioturbation signals in the soil. Although subsurface mixing is assumed to be the dominant process, there is a lack of data or methods to differentiate the effects of both bioturbation processes (Wilkinson et al., 2009; Halfen and Hasiotis, 2010; Michel et al., 2022).

45 Luminescence emitted by quartz and feldspar grains has successfully been used as tracer for bioturbation (Heimsath et al., 2002; Madsen et al., 2011; Stockmann et al., 2013; Johnson et al., 2014; Gliganic et al., 2015; Hanson et al., 2015; Reimann et al., 2017; Román-Sánchez et al., 2019a). The luminescence signal accumulates over time due to ionizing radiation emitted from radionuclides of elements within the uranium and thorium decay chains, as well as potassium-40, which are present in the soil, and due to cosmic rays. The luminescence signal is reset (bleached) when a soil particle is exposed to daylight. Thus,

50 the luminescence signal is a proxy for the residence time of soil particles in the subsurface and is ideally measured on single grains when used as a tracer for soil mixing (Duller, 2008). The distribution of the luminescence signal of different grains in a sample informs about the type and intensity of the mixing process (Bateman et al., 2003, 2007). Moreover, their changes with depth provide additional information on rates, patterns and intensity of bioturbation.

Luminescence signals are often used in combination with numerical or analytical tools to calculate particle ages and soil mixing

55 rates, and characterize mixing patterns (Schiffers et al., 2011; Furbish et al., 2018a, b; Román-Sánchez et al., 2019b; Gray et al., 2020; Yates et al., 2024). These tools are often based on a single diffusion-based implementation of the mixing process, which limits the possibilities to separate mixing signals by different biota (Schiffers et al., 2011), or are based on models stemming from aquatic ecology without adequate testing for terrestrial environments (Michel et al., 2022). Recent developments in soil-landscape evolution modelling enable the integration of luminescence tracers with process-based

60 simulations of soil and landscape processes (ChronoLorica model; van der Meij et al., 2023). This integration enables the simulation of the effects of different bioturbation processes on luminescence-depth profiles, which can help to quantify the

impacts of different bioturbation processes on soil mixing, better formulate bioturbation processes and their effects on nutrient cycling and other soil functions (Creamer et al., 2022), simulate soil mixing over different spatial and temporal scales (e.g., Schiffers et al., 2011) and provide a stronger role of biota in soil-landscape evolution models (Meng et al., 2022).

65   The objective of this study is to provide qualitative and quantitative tools for differentiating the impacts of mounding and subsurface mixing during soil bioturbation using luminescence tracers. By integrating experimental luminescence-based bioturbation datasets with soil evolution modelling, we aim to 1) characterize typical luminescence-depth profiles for mounding and subsurface mixing, 2) determine how varying parameters and combinations of these processes affect these depth profiles and 3) derive quantitative process rates and contributions from experimental data through model calibration.

2   Methods

2.1   Conceptual models of soil mixing

Mounding and subsurface mixing have distinct effects on the soil and luminescence tracers. In this section, we conceptually discuss these effects as a basis for their numerical implementation.

Soil bioturbation by *mounding* causes a net upward transport of soil material to the soil surface (Figure 1A). This soil material
75   is mined from previously buried material from the upper part of the soil (~ 1 m for termites, Kristensen et al., 2015), effectively leading to recycling of soil material in the mounding process over longer timescales. This recycling exposes a large part of the soil grains to daylight, leading to only a limited amount on non-surfaced grains that can carry a saturated luminescence signal. Typical mounding organisms are gophers, moles and termites (Gabet, 2000; Wilkinson et al., 2009; Kristensen et al., 2015). Mounding rates most likely decrease with depth due to decreasing biotic activity (Gray et al., 2020).

80   The diffusion-like transport caused by organisms that perform *subsurface mixing* moves soil material in between subsurface layers (Figure 1B). Typical mixing organisms are endogeic and anecic earthworms which (partly) live underground (Taylor et al., 2019), ants and subterranean termites that create subsurface galleries (Richards, 2009; Halfen and Hasiotis, 2010; Rink et al., 2013; Stewart and Anand, 2014; Taylor et al., 2019) and tree roots that shift material around when growing and which leave pores that can be filled with material after decay of the root material (Johnson et al., 2014; Ruiz et al., 2015). With
85   subsurface mixing, there is much smaller proportion of grains that is transported to the surface, leaving a higher proportion of non-surfaced grains. Also, for subsurface mixing, mixing rates probably decrease with depth, due to decreased biotic activity (Figure 1B).
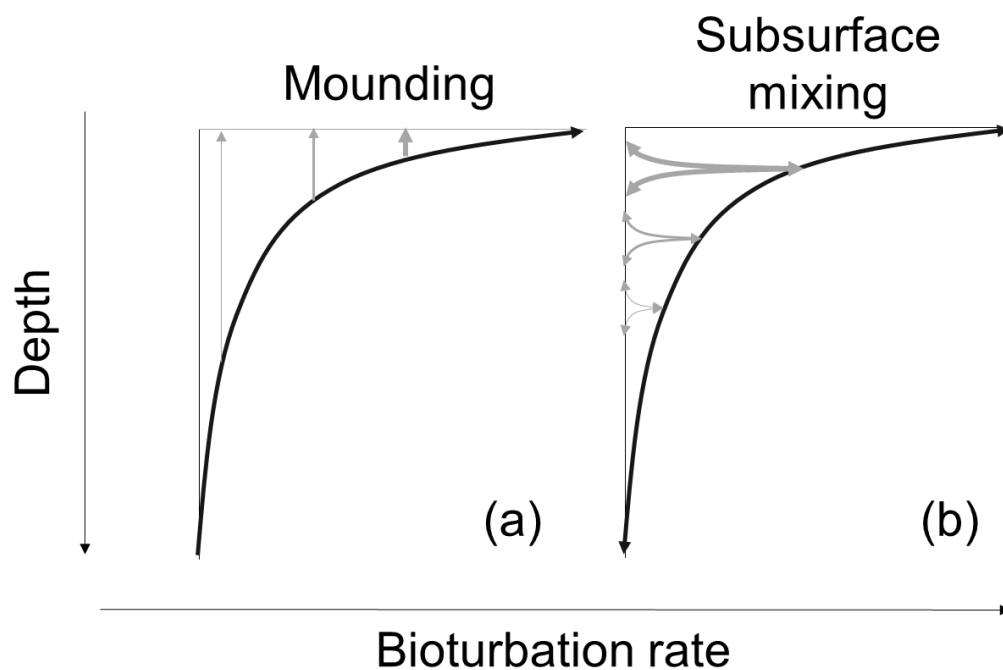
Figure 1: Conceptual drawing of mounding and subsurface mixing. Subsurface mixing and mounding are visualized here with an exponential depth function (see Sect. 2.3.2). The arrows indicate direction and their thickness the intensity of soil transport.

2.2   Experimental studies

We compiled three quartz and feldspar single-grain luminescence-based datasets of soil mixing by different organisms to characterize luminescence-depth profiles (Table 1). The main bioturbating organisms are termites who preferentially mound (Kristensen et al., 2015), anecic earthworms who both mound and mix the subsurface (von Suchodoletz et al., 2023) and ants who mainly mix the subsurface (Román-Sánchez et al., 2019a). All measurements were performed using Risø TL/OSL DA15 and DA20 luminescence readers equipped with ^{90}Sr/^{90}Y beta sources. The luminescence signals of single-grain quartz for the termites study were stimulated using a green laser for single grains (Kristensen et al., 2015). The signals were detected by a UV-sensitive photomultiplier tube (PMT) through a 7.5 mm Schott U-340 filter. K-rich feldspars were stimulated using an IR laser and the signals were detected with a LOT/ORIEL D410 interference filter (Román-Sánchez et al., 2019a; von Suchodoletz et al., 2023). Details regarding the sample preparation and the exact measurement conditions are given in the respective publications and a summary is provided in Table 1.

Table 1: Overview of experimental single-grain luminescence datasets used in this study. Q = Quartz, FSP = Feldspar, SG = single grains, Post-IR IRSL = Post-infrared infrared stimulated luminescence, PH = preheat

Organism	Primary mixing process	Reference	Selected profile	Active mixing depth	Defined bioturbation period or saturation criteria	Luminescence method
Termites	Mounding	(Kristensen et al., 2015)	Unit II	1.02 m	< 4 ka, onset of deforestation and start of savannah ecosystem	Q, SG, OSL, grain size: 90-180 μm, OSL
Anecic earthworms	Subsurface mixing and mounding	(von Suchodoletz et al., 2023)	Profile 2	60 cm	< 13.2 ka, estimated start of bioturbation by earthworms > 3.8 ka, end of bioturbation, due to burial of soil below burial mound	FSP SG, post-IR$_{50}$IRSL$_{150}$ (PH 175 °C, 60 s), grain size: 212-250 μm
Ants	Subsurface mixing	(Román-Sánchez et al., 2019a)	SC-10	50 cm	2*D$_0$ (Wintle and Murray, 2006)	FSP SG, post-IR$_{50}$IRIRSL$_e$ (PH 200 °C, 60 s), grain size: 212-250 μm

105 From these datasets, we are only interested in the ages of grains that have been bioturbated by the current dominant bioturbating agent. For the termites and worms datasets, there is a defined time period in which the current agent has been and continues to be active (Table 1). Grains falling outside of this timeframe are filtered out and excluded from our analysis of age distributions. Instead, we incorporate this fraction of particles ($f_{filtered}$) with the fraction of grains that have not reached the surface at all and have a saturated luminescence signal ($f_{non-surfaced}$). The remaining fraction (f_{bio}) contains the grains that have reached the surface

110 through bioturbation by the current dominant agent (Eq. (1)). f_{bio}, or the bioturbated fraction, is similar to the non-saturation factor (NSF) as defined by Reimann et al. (2017), with the addition of another rejection criterion based on the bioturbation period.

$$f_{bio} = 1 - \left(f_{non-surfaced} + f_{filtered} \right) \tag{1}$$

2.3 Simulations

115 ### 2.3.1 Model description

The bioturbation simulations are performed in the model ChronoLorica (Van der Meij and Temme, 2022; Van der Meij et al., 2023), which is an extension of the soil-landscape evolution model Lorica (Temme and Vanwalleghem, 2016; Van der Meij et al., 2020). Lorica is a mass-based four-dimensional numerical model that simulates the development of terrain and soil properties due to various geomorphic and pedogenic processes. The landscape is represented by a raster, where every raster

120 cell contains a pre-defined number of soil layers. The layers contain a mass of five mineral soil textures (coarse, sand, silt, clay and fine clay) and two organic matter types (young and old). Throughout the simulations, the contents of the layers change due to the addition, removal or transformation of the soil material by the simulated processes. Changes in the mass composition

of each layer are translated to changes in layer thickness and surface elevation through the bulk density. Lorica works with dynamic layer thicknesses, enabling easy calculation of additions and subtractions from each layer. The layers start with a pre-
125 defined initial thickness. When a layer thickness becomes more than 55% thicker than the initial thickness, the layer splits into two new layers. When a layer thickness becomes thinner than 55% of the initial thickness, the layer is merged with a neighbouring layer.

The ChronoLorica extension couples the pedogenic and geomorphic processes in the model to several geochronometers. In this study, we use soil particle burial ages, akin to luminescent grains, as tracer for bioturbation. We term these *luminescence*
130 *particles* in this study. These particles act similarly to grains of sand-sized quartz or feldspar in real soils. Their age increases during their time of burial. When the particles are transported into the surface layer, their age is reset. This surface layer has a fixed depth that represents the bleaching depth. The transport of luminescence particles is coupled to the transport of the sand fraction of the model, which is the texture class that is typically used for single-grain luminescence dating (Duller, 2008). Due to memory constraints in the model, the number of tracked luminescence particle ages is much lower than the number of sand
135 particles present in each layer. Therefore, we used a probabilistic approach to determine whether a luminescence particle is transported together with the sand from one layer to another. The transport probability for each individual particle is determined by dividing the transported mass of sand out of a source layer by the total mass of sand present in that source layer (Eq. (2)).

$$P_{transport} = \frac{sand\ transported\ [kg]}{total\ sand\ present\ [kg]} \tag{2}$$

2.3.2 Depth functions

140 Bioturbation is most likely a depth-dependent process, but whether the mixing rates decrease linearly or exponential with depth is still unknown (Gray et al., 2020). In our simulations, we consider three typical depth functions for changes in bioturbation rate that describe how the bioturbation rate changes with increasing soil depth (Minasny et al., 2016; Figure 2). These depth functions can be applied to both bioturbation processes. The depth functions describe i) a linear decrease with depth (*gradational*, Eq. (3)), ii) an exponential decrease with depth (*exponential*, Eq. (4)) and iii) a uniform mixing rate, which
145 reduces abruptly to zero below the mixing zone (*abrupt*, Eq. (5)). In these equations, the bioturbation rate at depth z $(BT(z))$ [kg m^{-2} a^{-1}] is controlled by the potential bioturbation rate BT_{pot} [kg m^{-2} a^{-1}] and a depth decay parameter (dd_{grd}, dd_{exp}, dd_{abr}) [m^{-1}] that determines the shape of the depth function.

$$BT(z) = \begin{cases} BT_{pot} * \left(1 - dd_{grd} * z\right), & z \leq \frac{1}{dd_{grd}} \\ 0, & z > \frac{1}{dd_{grd}} \end{cases} \tag{3}$$

$$BT(z) = BT_{pot} * \left(1 - e^{-dd_{exp} * z}\right) \tag{4}$$

150
$$BT(z) = \begin{cases} BT_{pot}, & z \leq dd_{abr} \\ 0, & z > dd_{abr} \end{cases} \tag{5}$$

The part of BT_{pot} that occurs in one layer (BT_{layer}) is determined by calculating the integral of the bioturbation depth function from the upper to the lower depth (z_{upper}, z_{lower}) of the respective layer, and divide this by the integral over the entire depth function (Eq. (6)). The integral over the entire depth function is limited to depth z_{lim}, which represents the active mixing depth and determines where the bioturbation stops. This is $1/dd_{grd}$ for the gradational function, the total soil depth sd for the exponential function, where $z \leq sd$, and dd_{abr} for the abrupt function.

$$BT_{layer} = BT_{pot} * \frac{\int_{z_{upper}}^{z_{lower}} BT(z)dz}{\int_0^{z_{lim}} BT(z)dz} \tag{6}$$
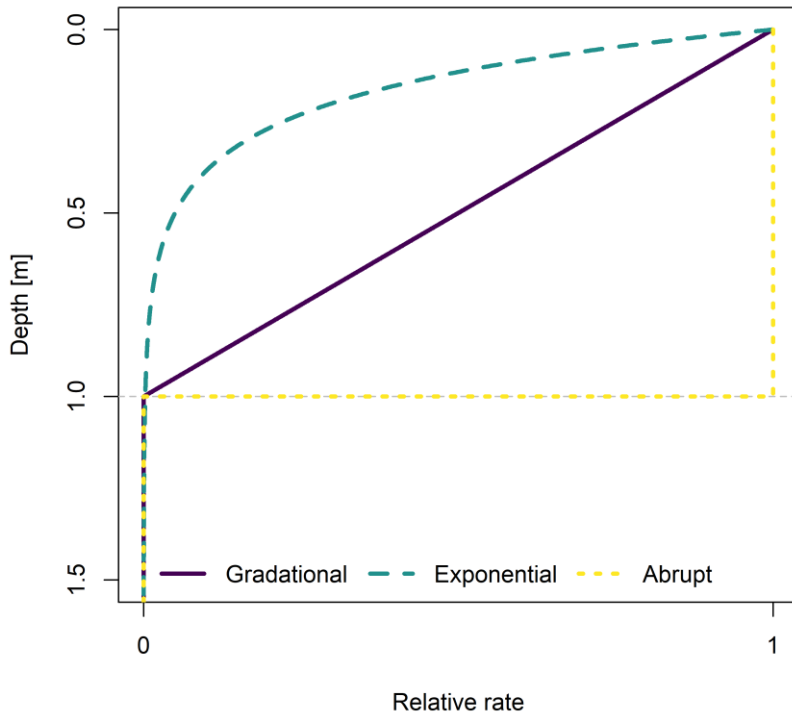
Figure 2: Depth functions that are used for bioturbation simulations. The depth functions determine how bioturbation rates change with soil depth. The parameters are selected, so that all bioturbation effectively occurs in the top 1 meter of the soil (grey-dashed line).

2.3.3 Process descriptions

We simulate the mounding process as upward transport of soil material from the subsurface. Eq. (6) determines how much material is taken from each soil layer. This material is then transported to the surface layer, gradually burying previously mounded material. In this implementation, the development and erosion of surface mounds is simplified into generation of a new surface layer, that results from the mound erosion.

The subsurface mixing process is simulated by an exchange of soil material between all present soil layers. Eq. (6) determines how much material each soil layer (donor layer) can exchange in total with all other exchange layers in the profile. The exchange $BT_{exchange}$ between the donor layer and all other layers is controlled by Eq. (7). This equation integrates an exponential equation that starts at the centre thickness of the donor layer (z_{layer}), over the upper and lower depths (z_{upper}, z_{lower}) of the exchange layer. This integral is divided by the sum of the integral of two other exponential equations, starting from z_{layer} and going towards the soil surface and the bottom of the soil profile (sd). The gradient of these exponential equations is controlled by depth parameter dd_{mix} [m^{-1}].

$$BT_{exchange} = BT_{layer} * \frac{\left| \int_{z_{layer}-z_{upp}}^{z_{layer}-z_{lower}} e^{(-dd_{mix}*z)} dz \right|}{\int_0^{sd-z_{layer}} e^{(-dd_{mix}*z)} dz + \int_0^{z_{layer}} e^{(-dd_{mix}*z)} dz} \tag{7}$$

2.3.4   Model set-up

We simulate the mixing processes in a 2 m deep, one-dimensional soil profile (pedon). The pedon contains 200 soil layers of 1 cm thick, with an upper layer of 5 mm representing the bleaching depth. The bleaching depth is based on model-based estimates (Furbish et al., 2018b) and is in line with light penetration depths in rocks (0-15 mm, Meyer et al., 2018).. We simulate a uniform loess-like soil texture (25% sand, 60% silt, 15% clay) with a constant bulk density of 1500 kg m^{-3} to avoid effects of textural and density variations on the age distributions in the simulations. The simulations start with 150 luminescence particles per soil layer. Each simulation ran for 10 ka with a step size of one year.

We simulated different scenarios to show how age-depth profiles change due to varying bioturbation processes and model parameters (Table 2). Except when indicated differently in Table 2, each scenario ran with a gradational depth profile and a potential bioturbation rate (BT_{pot}) of 10 kg m^{-2} a^{-1} (loosely based on rates reported in Wilkinson et al., 2009: 0.3-110 kg m^{-2} a^{-1}). The depth decay parameters were selected such that bioturbation is restricted to the upper 1 meter of the pedon (Figure 2; dd_{grd}: 1 m^{-1}, dd_{exp}: 6 m^{-1}, dd_{abr}: 1 m^{-1}, dd_{mix}: 10 m^{-1}). These parameters were selected to illustrate how bioturbation affects luminescence-based depth profiles and need to be constrained with experimental data, or through inverse modelling, when applied to real-world settings.

Table 2: Simulation scenarios in this study. The simulated mixing processes and the variations in the model parameters are indicated.

Scenario	Process	Variations in model parameters
1	Mounding	Different depth functions (gradational, exponential, abrupt)
2	Subsurface mixing	Different depth functions (gradational, exponential, abrupt)
3	Mounding	BT_{pot} (1-10 kg m^{-2})
4	Subsurface mixing	BT_{pot} (1-10 kg m^{-2})
5	Mounding + subsurface mixing	Relative contribution of processes (0-100%)

2.4   Data presentation and comparison

190   Because we expect non-normal distributions in the data, we use probability functions to represent the age distributions. We calculate these functions using a bandwidth following the method of Sheather and Jones (1991), which was developed for non-normal distributions. Saturated or non-bleached grains were excluded from the probability functions. We present our results using three metrics derived from the luminescence-based depth profiles:

- The modal age of the probability function, as the most likely age;

195   - The interquartile range, as a measure of the width of the distribution;

- The bioturbated fraction(f_{bio}, Eq. (1)), as a measure of the fraction of bleached particles.

For the comparison of experimental data and simulations, we normalized the depths and luminescence ages. For the experimental data, we normalized depths by dividing sampling depth by the maximum sampling depth and the luminescence ages by dividing the individual grain ages by the extent of the bioturbation period (Table 1), or by the maximum age in the 200   dataset if the former wasn't defined. For the simulations, the depth was normalized by dividing simulation depth by the active mixing depth of 1 m. The simulated ages were normalized by dividing by the simulation time of 10 ka.

3   Results

3.1   Experimental studies

Figure 3 shows the luminescence-based depth profiles from the experimental datasets. The plots are in order of increasing 205   contribution of subsurface mixing (termites -> worms -> ants). With a larger contribution of subsurface mixing, the interquartile ranges increase and the bioturbated fractions decrease. The termites and worms datasets show clear age-depth trends, while the ants dataset shows a more scattered depth profile with a discontinuity in the modes. The termites and ants datasets show an increasing interquartile range with depth, while the worms dataset shows relatively constant interquartile range. There are also clear differences in the bioturbated fraction. The termites dataset has a bioturbated fraction over 50% for 210   the entire profile with over 90% bleaching in the upper 60 cm. The worms dataset also has a well-bleached upper sample, but the bioturbated fraction approaches 25% for the lowest sample. For the ants, only the upper sample shows good bleaching, with a bioturbated fraction of 97%. This drops to 12% and 6% deeper in the profile, where only 6 to 8 samples contain a luminescence signal.
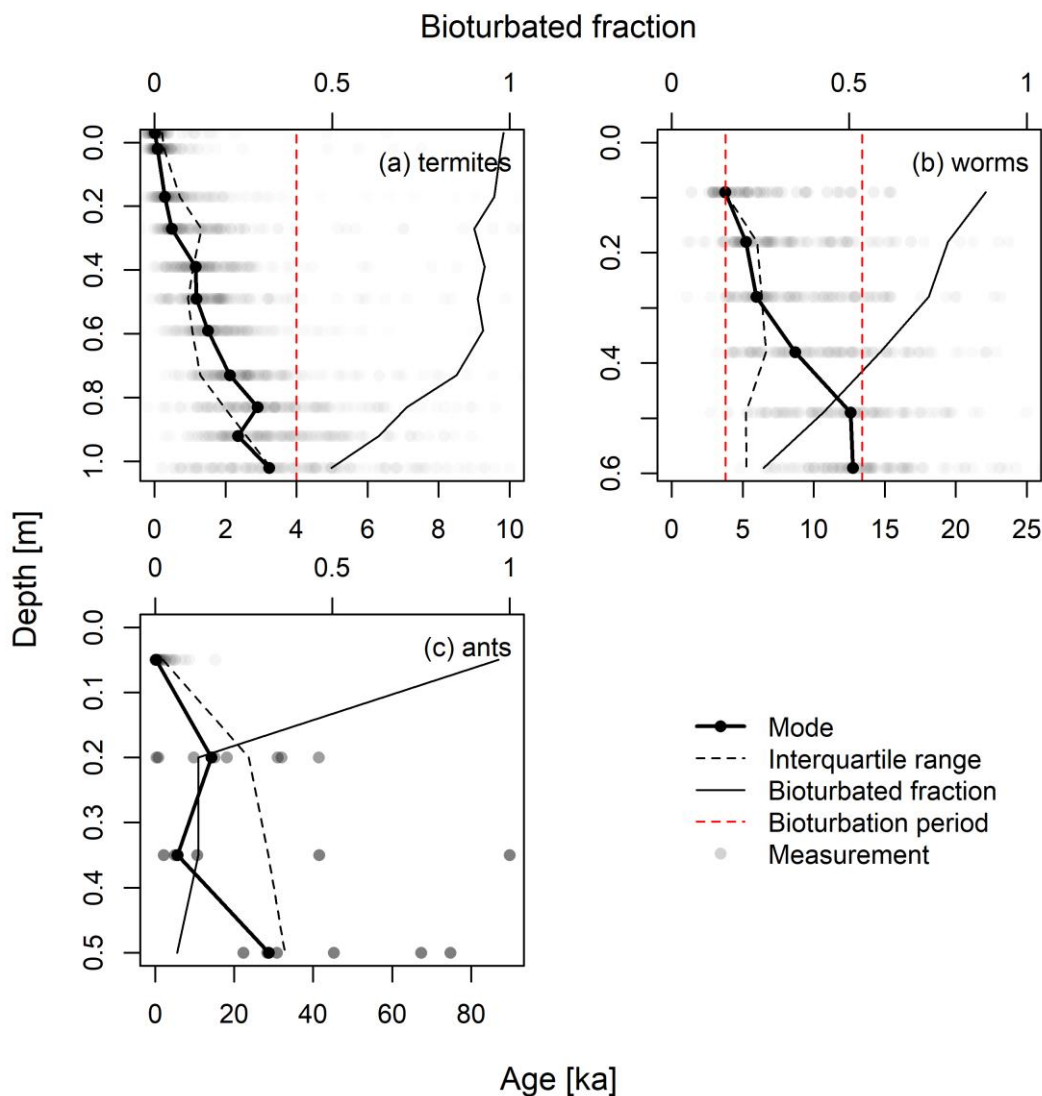
Figure 3: Age-depth profiles for the experimental datasets used in this study. The bottom axes show the ages of the measurements. The upper axes show the bioturbated fraction. Where provided, the red dashed line indicates the period of bioturbation by the current agent (Table 1).

3.2 Comparison of depth functions and bioturbation rates

The simulations of separate mounding and subsurface mixing processes with varying depth functions show in clear differences in the resulting depth profiles (Figure 4). The mounding shows curved age-depth trends with low interquartile ranges for all different depth functions, which slightly increase closer to the lower boundary of the active mixing zone of 1 m (Figure 4A). The gradational and exponential profiles approach the simulation time of 10 ka at the bottom of the profile, while the abrupt profile has much younger ages and a steeper depth profile. For each depth profile, almost all particles have been bioturbated

and bleached in the active mixing zone, as shown by the bioturbated fraction. Below this zone, none of the particles are
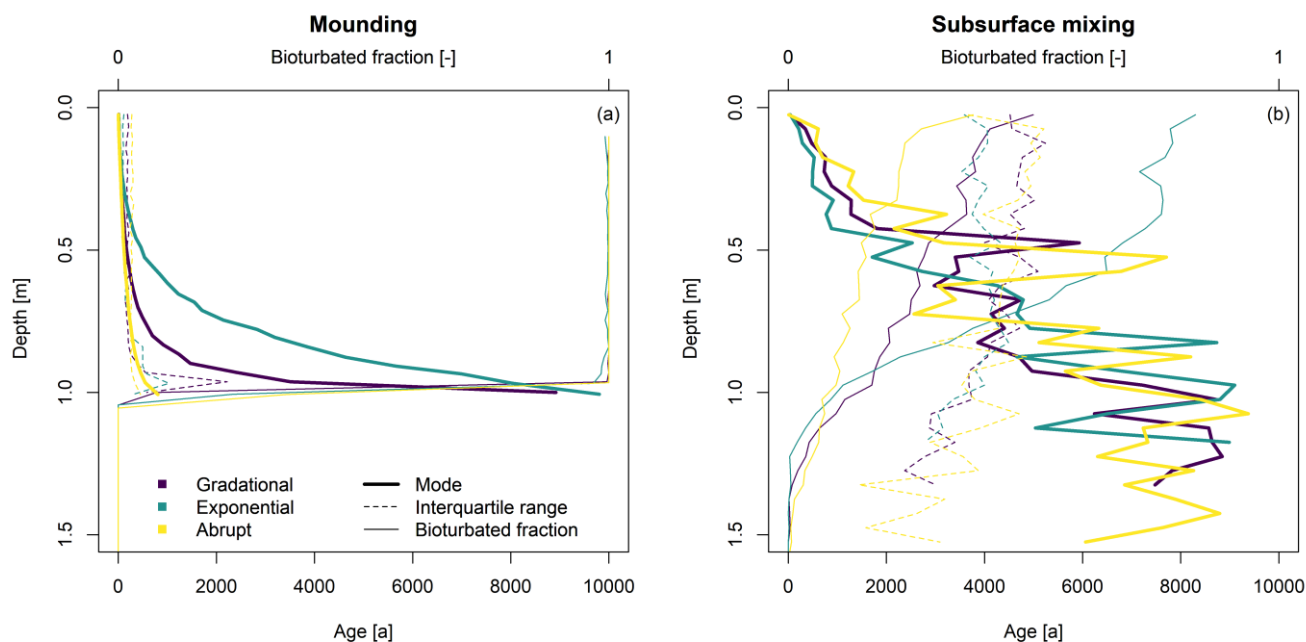
225   bioturbated.

Figure 4: Luminescence-based depth profiles resulting from simulations of (A) mounding and (B) subsurface mixing, using different depth functions, with potential bioturbation rates of 10 kg m⁻² a⁻¹.

In contrast, the simulations of subsurface mixing show more chaotic, scattered age-depth profiles that only show a general

230   increasing trend with depth (Figure 4B). This scatter also increases with depth and even reaches below the active mixing zone of 1 m, due to exchange of material from bioturbated layers with all other soil layers. The modes are similar for each simulated depth function, with slightly lower interquartile ranges for the upper part of the exponential depth profile. The interquartile ranges are high for all simulations, and generally decrease down the profile. This concerns only a small number of particles, as evidenced by the bioturbated fraction. The amount of bioturbated particles decreases with soil depth. The exponential profile

235   contains most bioturbated particles, followed by the gradational and abrupt profiles.

Variations in the bioturbation rate for the mounding and subsurface mixing processes shows a clear effect on the steepness of the age-depth curves (Figure 5). For the mounding process, higher rates lead to a steeper age-depth profile. Throughout the bioturbated profiles, almost all luminescence particles have been bleached, independent of the rate. For the subsurface mixing process, higher rates show younger modal ages and higher bioturbated fractions. The interquartile ranges show comparable

240   trends, with different levels of scatter. Bioturbation rates also affect the depth of the mixed profiles, where lower bioturbation rates lead to shallower mixing bioturbated profiles.
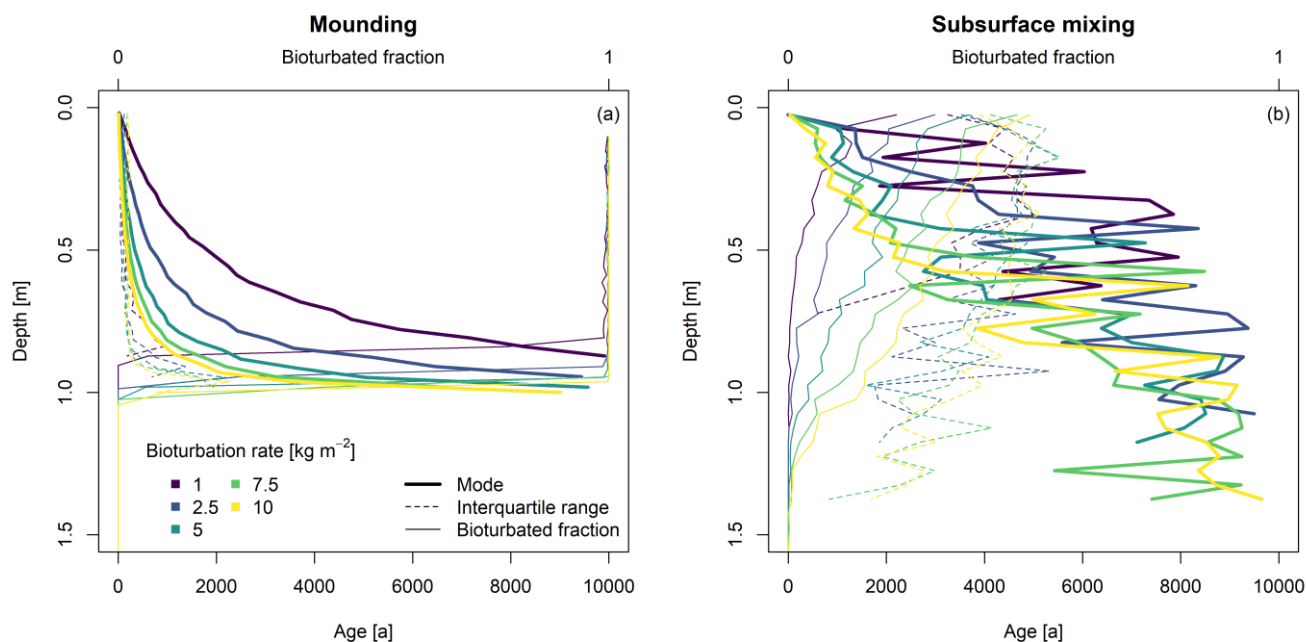
Figure 5: Age-depth profiles resulting from bioturbation by A) mounding and B) subsurface mixing, using a gradational depth profile and varying bioturbation rates.

3.3   Combination of mounding and subsurface mixing

Simulations where mounding and mixing were combined in different ratios show that the mounding process dominates the age-depth characteristics (Figure 6A). Only when the fraction of mounding decreases to less than 5%, the depth curves start to turn towards the profile with solely subsurface mixing. The same pattern is visible for the bioturbated fraction, but the interquartile range reacts quicker to changes in the ratio of mounding and subsurface mixing. Overall, a larger contribution of subsurface mixing leads to older luminescence particles in the profile (Figure 6A), wider age distributions (Figure 6B) and less bioturbated particles (Figure 6C).

The general trends in the experimental data conform with the trends in the simulation data. Termites, as mounding organisms, show lower modes of ages compared to worms, which both mound and mix (Figure 6A). The ants show lower modes of ages than both other organisms, but this can be attributed to the normalization procedure: while the observed period of bioturbation had been constrained in case of the termites and worms dataset, the ants dataset had no such constraint and was consequently normalized by much higher age values (Table 1). The experimental datasets show increasing interquartile ranges with a larger contribution of subsurface mixing, with deviations from the trends in the simulated data mainly in the topsoil (Figure 6B). Also in this case, the ants dataset forms the exception due to the high normalization age. The simulated interquartile ranges are much lower for mounding-dominated scenarios than the experimental studies, indicating an underestimation of the spread in age distributions. The bioturbated fraction also shows clear differences between mounding and subsurface mixing organisms, with a higher proportion of bioturbated grains for mounding organisms (Figure 6C).
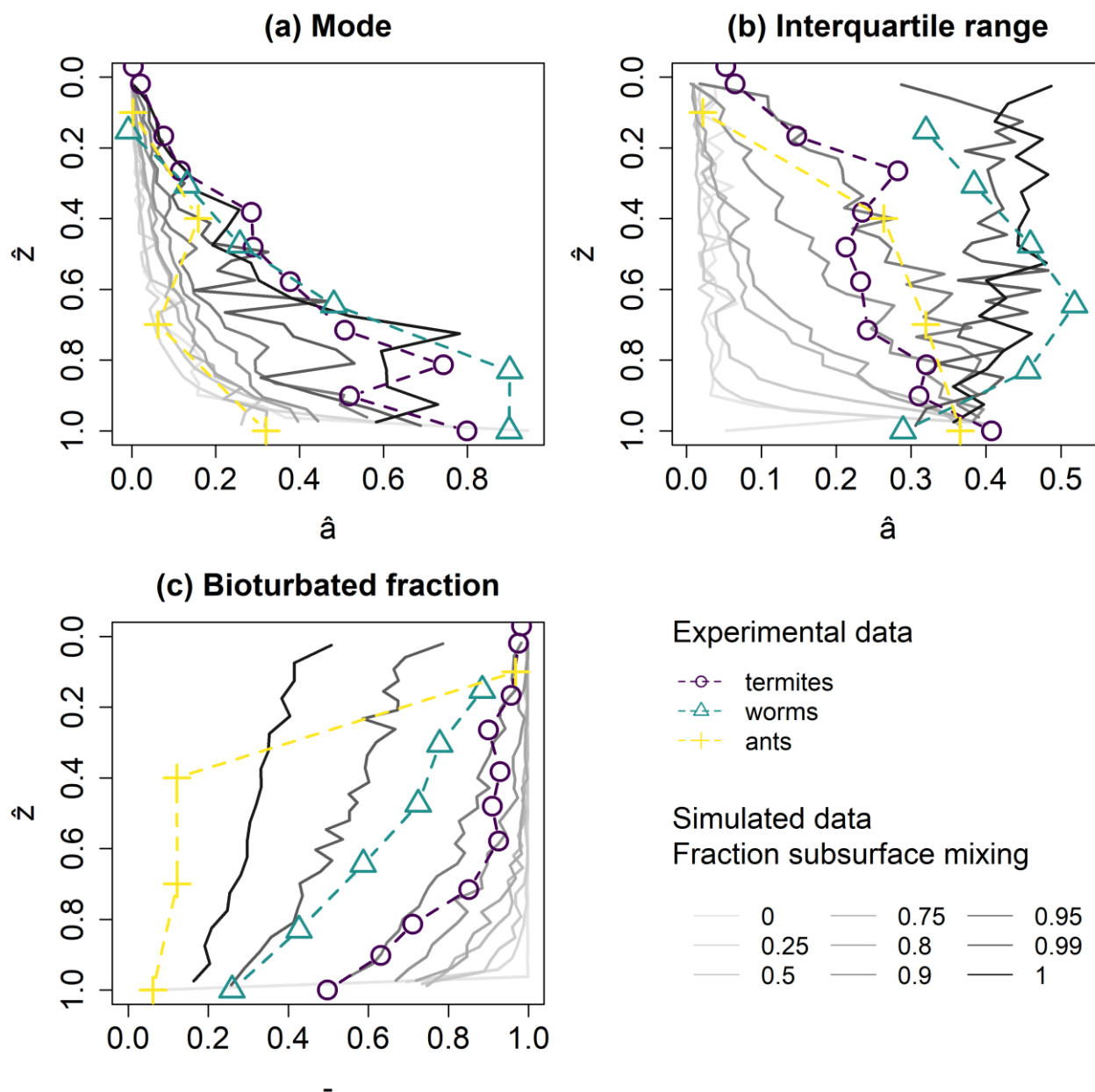
Figure 6: Statistics for mixes between mounding and subsurface mixing (grey lines), aggregated per 5 soil layers (~ 5 cm), compared to the experimental datasets (coloured lines and points). Results were normalized for age (â) and depth (ẑ). The different windows show different statistics: A: mode of age distributions; B: interquartile range; C: bioturbated fraction. The simulations were run with a gradational depth function and active mixing zone of 1 m, with a total bioturbation rate of 10 kg m⁻² a⁻¹, divided over the two processes.

265

4   Discussion

4.1   Mixing patterns by mounding and subsurface mixing

270   Bioturbation induces different mixing patterns in the soil, depending on the organism and process. By the integration of luminescence tracers and numerical simulations, we identified distinct ways in which different processes and parameters impact soil mixing. Here, we will elaborate on the processes, their effects on luminescence tracers and show that they are consistent across experimental datasets.

The upward advective transport of soil material by mounding animals continuously buries previously mounded material, which
275   leads to age-depth profiles in the active mixing zone that resemble depositional profiles. The continuous upward transport of material to the surface results in a high degree of bleaching and consequently narrow age distributions, as evidenced by the termites dataset and the numerical simulations (Figure 3A; Figure 4A). The lower boundary of the active mixing zone is often characterized by an abrupt increase in ages, changing widths of age distributions, lower age-depth rates and a decrease in the bioturbated fraction. This is clearly visible in the termites study by Kristensen et al. (2015), where the fraction of saturated
280   grains increases from 0–4 % in the active mixing zone to up to 60% in the layers below (data not shown), accompanied by a jump in the luminescence ages and increase in the uncertainties. The same is visible in the data from Madsen et al. (2011), who measured luminescence-based age-depth curves from aliquots collected in tidal flats, which are bioturbated by mounding lugworms. There is a clear distinction between the active mixing zone, with narrow age distributions and steeper age-depth gradients, and the underlying depositional sequence.

285   The age-depth curves of bioturbation by subsurface mixing display completely different characteristics (Figure 6). The limited bleaching at the surface and diffusion-like transport leads to a low population of bleached particles in the subsurface and wide luminescence distributions. The stochastic nature of particle transport by subsurface mixing is clearly visible in the ants dataset (Figure 3C; Román-Sánchez et al., 2019a), with only few luminescent grains in the subsoil that show a high age range. Ants often create mounds at their nest entrances (Richards, 2009), suggesting that luminescence-based depth profiles for ants should
290   contain mounding signals as well. Román-Sánchez et al. (2019a) studied a profile on a hilltop with an equilibrium between soil erosion and soil production. If the erosion primarily removed the surface mounds, the subsurface mixing component of bioturbation would be amplified. The low bioturbated fraction and wide age distributions are also consistent in other luminescence datasets with considerable subsurface mixing components, for example by root activity (Heimsath et al., 2002; Stockmann et al., 2013; Johnson et al., 2014). Two of these datasets only contained a small proportion of non-saturated grains
295   (Heimsath et al., 2002; Stockmann et al., 2013). Surprisingly, the data of Johnson et al. (2014) had a very low number of saturated grains in their dataset, which they attribute to an aeolian input of bleached quartz grains.

In addition to the studied processes, there are various other forms of bioturbation such as upheaval, involving the sudden detachment, homogenization, and re-deposition of soil. For example, when a tree is uprooted, the soil from the root clump falls back into the pit (Gabet et al., 2003). Ploughing could also be considered upheaval. Here, a body of soil is efficiently detached,
300   turned over and redeposited, for example by a mouldboard plough (De Alba et al., 2004; Van der Meij et al., 2019). Upheaval

likely induces similar age-depth patterns as mounding, but depending on the frequency and mixing depth will have older ages and lower bioturbated fractions. Bioturbation by upheaval, and its interactions with mounding and subsurface mixing, will be explored in future research.

The distinct effects of different bioturbation processes on soil fluxes that we identified here emphasize the necessity of
305 including multiple formulations of bioturbation processes in soil evolution models and soil function models, as conventional diffusion-type subsurface mixing processes account for only a part of soil mixing.

4.2   Luminescence as tracer of soil mixing processes

Luminescence-based tracers rely on the exposure and bleaching of soil particles to daylight at the surface. Bleached particles are transported downward by various processes, where they can be measured as tracer for soil mixing. As a result, luminescence
310 primarily traces downward transport within soils (Gliganic et al., 2016). Luminescence-based age-depth profiles are predominantly influenced by mounding, because this process exposes more grains to daylight, and therefore do not adequately represent subsurface mixing processes (Figure 6A). The interquartile range, as proxy for the width of the age distributions, reacts quicker to changes in the balance of mounding and subsurface mixing (Figure 6B). This suggests that the interquartile range might be key in separating between mounding and subsurface mixing signals using luminescence-based tracers, which
315 is still one of the main challenges of determining bioturbation rates (Wilkinson et al., 2009; Halfen and Hasiotis, 2010). This will be explored further in Sect. 4.3.

The bioturbated fraction acts as a downward tracer of soil mixing due to supply of bleached grains from the surface, but can act as an upward tracer of soil mixing as well (Reimann et al., 2017). Bedrock weathering, increased bioturbation or surface denudation lead to the to the downward migration of the active mixing zone, introducing saturated grains from the bottom up
320 into the soil profile. These processes were not accounted for in this study. However, they do play a significant role in interactions between bioturbation and hillslope processes (Román-Sánchez et al., 2019b, a) and should be taken into account when applying bioturbation models in two to three-dimensional settings.

The modal ages, interquartile range and bioturbated fraction are not only influenced by the type of bioturbation processes, but also by the applied depth function and process parameters such as soil mixing rate. In Figure 7, we have compiled an overview
325 of how different processes, implementations and parameters affect the depth functions of luminescence-based metrics. The characteristics of these depth functions offer qualitative insights into the characteristics of the underlying mixing processes.
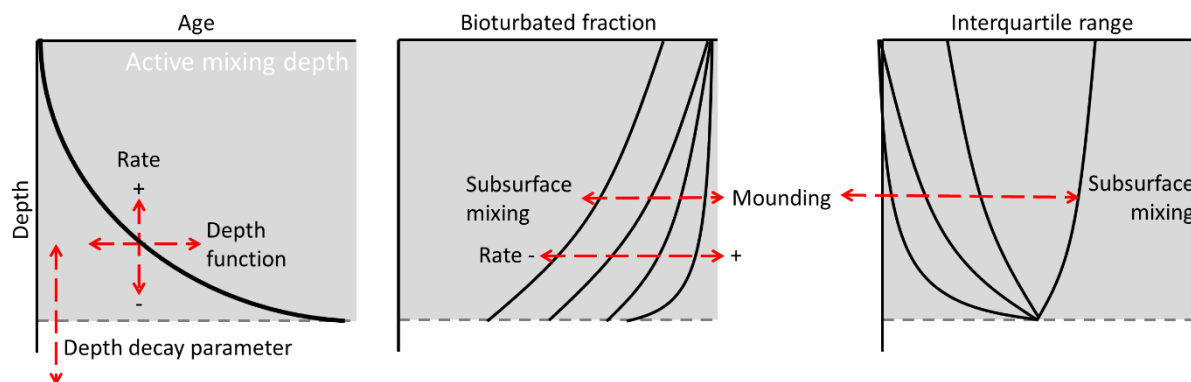
Figure 7: Conceptual overview of how different factors affect the depth profiles of luminescence-based metrics.

The majority of soil mixing happens in the active mixing zone, with the maximum depth being determined by the reach of
330   organisms into the soil (Figure 3), represented by the depth decay parameters in the simulations. This zone is distinguished
from underlying layers by younger, measurable ages and a higher bioturbated fraction. It is challenging to determine the depth
function of mixing processes from age-depth profiles. This supports earlier statements about determining depth dependency
of soil mixing (Gray et al., 2020). The steepness of the exponential age-depth profiles can either be a result of a different depth
function or a different soil mixing rate. The dominant mixing process can be derived from the bioturbated fraction and the
335   interquartile range, where a higher proportion of mounding results in higher bioturbated fractions and lower interquartile
ranges.

The combination of luminescence-based ages, the interquartile range and the bioturbated fraction provides a comprehensive
toolbox for tracing soil mixing processes. Ideally, these tracers are combined and verified with independent tracers that trace
either downward or upward transport. Fallout radionuclides or meteoric cosmogenic radionuclides are examples of downward-
340   oriented tracers (Tyler et al., 2001; Kaste et al., 2007; Johnson et al., 2014), while in situ created cosmogenic nuclides
(Heimsath et al., 1997; Brown et al., 2003) and reworked clay coatings originating from Bt horizons (papules, Miedema and
Slager, 1972; Sauzet et al., 2023) are produced in or below the soil column and therefore can act as upward-oriented tracers.
Numerical methods such as ChronoLorica provides a flexible platform to integrate different soil mixing tracers and simulate
their distribution in complex multi-mixed environments.

345   **4.3**   **Towards a quantitative evaluation of luminescence-based depth profiles**

This qualitative understanding of the luminescence-based depth profiles, coupled with a model capable of simulating various
bioturbation processes, sets the stage for a quantitatively determining the impact and rates of different bioturbation processes
through model calibration. Here we make a first attempt at this calibration for the termites and worms datasets, using the
accompanying model Mixed Signals (See Sect. 4.4). We do not attempt a calibration for the ants dataset, because the effects
350   of erosion and soil formation on this profile are not sufficiently constrained in the model.

16

There are several parameters in the model that need to be estimated or calibrated prior to a successful application. These parameters can be grouped in environmental parameters (type of mixing processes, depth of active mixing zone, bioturbation period), model-based parameters (bleaching depth, bleaching efficiency) and process-based parameters (bioturbation rate, ratio between contributing processes, depth function, depth decay parameters). For this calibration, we based the environmental

355 parameters on field observations and experimental results (Table 1) and used the same values as in the simulations above for the model-based parameters. In this first attempt we use the same depth decay parameters for the exponential depth profile and subsurface mixing as in the simulations above, but for actual bioturbation calibration, these parameters should be calibrated as well.

To determine the process-based parameters, we ran the model with varying depth functions, potential bioturbation rates and

360 contributions of mounding and subsurface mixing. We determined the parameter set that produced the closest match with the experimental data by minimizing the combined squared error ($error_{squared}$) of experimental and simulated modal age, interquartile range and bioturbated fraction (Eq. (8), where P are the different luminescence metrics and O is the number of observations in the experimental dataset.

$$error_{squared} = \sum_{p=1}^{P} \sum_{o=1}^{O} \left(p(o_{simulated}) - p(o_{experimental}) \right)^2 \qquad (8)$$

365 Calibration across all three metrics enabled us to capture the majority of the dynamics observed in the depth profiles resulting from different processes and parameters (Figure 7). To ensure equal weighting of the three metrics, the ages were normalized by dividing them by the runtime (i.e. bioturbation period) of the model. Consequently, all metrics have potential values ranging from 0 to 1.
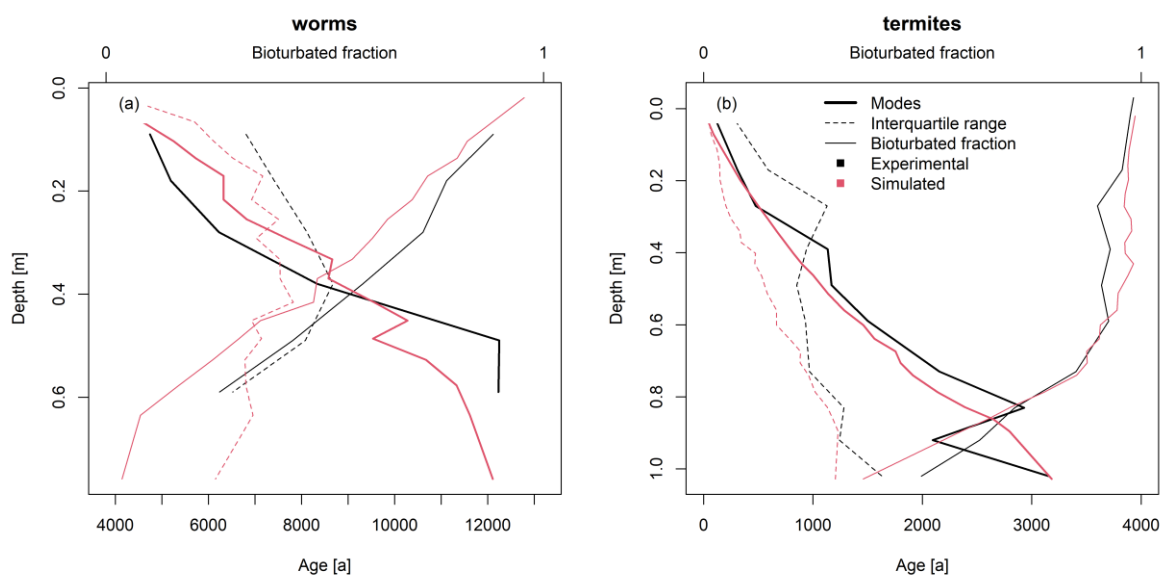
370 **Figure 8: Calibration results for the worms and termites datasets. Initial layer thicknesses in the model were 2 cm. To reduce scatter in the visualization of the model results stemming from the stochastic particle transport process, the simulated results (in red) are aggregated per three layers, resembling typical 5-cm thick OSL samples.**

The model is well equipped to reproduce the experimental depth profiles (Figure 8). The simulated depth profiles of the three metrics approach the experimental depth profiles, with some deviations due to fluctuations in the experimental data and the

375   calibration on three different metrics. For the worms dataset, the best matching parameters were a gradational depth profile, potential bioturbation rate of 1.5 kg m^{-2} a^{-1}, 90% subsurface mixing and 10% mounding. This ratio of processes agrees well with our expectations for burrowing anecic earthworms, which mainly live underground and sometimes visit the surface (Taylor et al., 2019). The parameter set that gave the best results for the termites dataset was an abrupt depth profile with a bioturbation rate of 4.5 kg m^{-2} a^{-1}, with 80% subsurface mixing and 20% mounding. We expected a much higher contribution

380   of mounding for the termites due to their construction of large surface mounds. However, a component of subsurface mixing was also expected, as termites transport material in the subsurface when they mine material for their mounds, similar to ant subsurface galleries (Rink et al., 2013). The abrupt depth profile that was calibrated for the termites data contradicts the findings of Gray et al. (2020), who found that mixing rates generally decrease with depth.

Interestingly, the calibrated bioturbation rates are multiple orders of magnitude larger than the soil reworking rates reported in

385   the original studies (~40 g m^{-2} a^{-1} for termites, Kristensen et al., 2015; ~20 - 80 g m^{-2} a^{-1} for worms, von Suchodoletz et al., 2023). These reported rates were based on measured OSL ages and their depths. These ages represent the current burial ages of the grains, but do not account for previous resurfacing of grains or subsurface transport without bleaching. Hence, they represent only the net displacement of soil particles from the surface to the subsurface. The calibrated rates are in the same order of magnitude as rates of mounding and mixing determined by earthworm ingestion rates and weighing worm casts and

390   surface mounds (see compilation in Wilkinson et al., 2009). Based on these factors, the actual bioturbation rates in the studied sites are probably closer to the calibrated rates than to the OSL-based soil reworking rates.

This modelling exercise provides unique opportunities to quantitatively distinguish mounding and subsurface mixing processes. However, the current results do not match with our expectations, especially for the termites dataset. This discrepancy is probably a consequence of the assumption of complete bleaching within the bleaching depth in the model. The bleaching

395   depth of 5 mm in this study was based on model-based estimates (Furbish et al., 2018b) and is in line with light penetration depths in rocks (0-15 mm, Meyer et al., 2018). However, in reality, not all near-surface grains are bleached, due to the attenuation of light after it penetrates the soil surface and the formation of soil aggregates, which shield inner particles from light. Notably, the agents responsible for soil mixing are also largely responsible for soil aggregation (Lee and Foster, 1991; Bottinelli et al., 2015). A lower bleaching efficiency – the fraction of particles that is bleached within the bleaching depth –

400   would result in lower bioturbated fractions and higher interquartile ranges, which are the same effects that a larger contribution of subsurface mixing has.

The bleaching depth and bleaching efficiency need to be better constrained before accurate calibration of the experimental profiles is possible. These model-based parameters could be estimated through model calibration, but this comes with the risk that multiple parameter combinations could result in equally plausible mixing scenarios, as bleaching efficiency and subsurface

405   mixing have similar effects on the calibration parameters. Experimental evidence on bleaching depths and bleaching efficiency

in soils, which likely vary across soil types and vegetation cover, is thus required to constrain these parameters and provide accurate, quantitative estimates of bioturbation rates and processes based on luminescence tracers and numerical modelling.

4.4 Simulation tool for bioturbation

The simulations presented in this paper were modelled with ChronoLorica, which is a comprehensive soil-landscape evolution model that simulates multiple pedogenic and geomorphic processes, together with multiple geochronometers (Van der Meij et al., 2023). The model, without the new formulations for bioturbation, is available via the Zenodo repository (Van der Meij and Temme, 2022).

We also developed a separate model, named Mixed Signals, which contains the formulations of bioturbation processes and their effects on luminescence tracers, as described in this paper, as well as visualization and calibration tools. This model can be used or adapted for simulating bioturbation effects on luminescence-based tracers, for example in explorative studies or for education purposes. The model is written in Julia, which is an interactive high-performance scientific computing language (Bezanson et al., 2017). The Mixed Signals model is freely available https://github.com/MarijnvanderMeij/Mixed-signals Bioturbation and will be published to the Zenodo repository after potential changes after review. The download contains the following files:

- a readme file with instructions to launch the model,
- a Jupyter Notebook with illustrative examples demonstrating how to use the model to simulate soil mixing and its effects on luminescence-based depth profiles,
- a script with all the functions that are required to run the model and create visualizations.

5 Conclusions

Soil bioturbation plays a crucial role in soil functions and soil evolution by cycling carbon and nutrients, but there is limited knowledge on how different mixing processes affect fluxes and rates of soil material. In this study, we combined experimental luminescence-based datasets and numerical modelling to study two main bioturbation processes – mounding and subsurface mixing – and their respective mixing patterns. These mixing patterns have distinct effects on luminescence tracers, which we characterized with three metrics: the modal age as most probable age of each layer, the interquartile range as measure of the width of the distributions and the bioturbated fraction as the fraction of bleached particles in each layer.

By numerically simulating mounding and subsurface mixing with varying rates, depth functions and interactions between processes, we determined how each process affects the luminescence-based depth profiles. Mounding is an advective process that moves soil material to the surface, leading to a high degree of luminescence signal resetting (bleaching), low interquartile ranges and a high bioturbated fraction. Subsurface mixing is a diffusive process, which transports a much lower number of grains at the surface, leading to leading to high interquartile ranges and low bioturbated fractions. We summarized these effects in a conceptual diagram to facilitate qualitative interpretation of luminescence-based depth profiles.

A first attempt to quantitatively interpret luminescence-based depth profiles through model calibration showed that the model is able to reproduce the experimental depth profiles and provide realistic bioturbation rates. The model is not yet equipped to accurately determine the relative contribution of mounding and subsurface mixing in the experimental datasets, likely due to the overestimating the degree of bleaching at the surface. Experimental data on bleaching depth and bleaching efficiency in soils is required before accurate, quantitative estimates of bioturbation rates and processes can be determined.

Our compilation of luminescence-based soil tracer studies and numerical simulations shows that bioturbation is more than a simple diffusive mixing process. Different organisms cause different transport processes in the soil, with major differences in fluxes of soil material and consequently nutrients and carbon. We provide numerical formulations of two main bioturbation processes, which could be used to improve soil function and soil evolution models. The accompanying model Mixed Signals contains these implementations and can be used for explorative studies, education purposes and quantitative determination of bioturbation parameters through model calibration.

Code and data availability

The luminescence data used in this study are published in earlier work (Kristensen et al., 2015; Román-Sánchez et al., 2019a; von Suchodoletz et al., 2023) and we refer to the authors of these works for data requests. The ChronoLorica model is publicly available via https://doi.org/10.5281/zenodo.7875033 (Van der Meij and Temme, 2022). The new bioturbation implementations can be found in the maintained versions of ChronoLorica and other versions of Lorica through https://github.com/arnaudtemme/lorica_all_versions (last access: 13 May 2024), and will be added to a new version of the model. The model Mixed Signals is available via https://github.com/MarijnvanderMeij/Mixed-signals_Bioturbation and will be published in the Zenodo repository after potential changes after review.

Author contributions

W. Marijn van der Meij: Conceptualization, Methodology, Software, Visualization, Writing – Original draft. **Svenja Riedesel**: Conceptualization, Investigation, Writing – Review & Editing. **Tony Reimann**: Conceptualization, Writing – Review & Editing.

Competing interests

The authors declare that they have no conflicts of interest.

Acknowledgements

References

470 Bateman, M. D., Frederick, C. D., Jaiswal, M. K., and Singhvi, A. K.: Investigations into the potential effects of pedoturbation on luminescence dating, Quaternary Science Reviews, 22, 1169–1176, https://doi.org/10.1016/S0277-3791(03)00019-2, 2003.

Bateman, M. D., Boulter, C. H., Carr, A. S., Frederick, C. D., Peter, D., and Wilder, M.: Preserving the palaeoenvironmental record in Drylands: Bioturbation and its significance for luminescence-derived chronologies, Sedimentary Geology, 195, 5–19, https://doi.org/10.1016/j.sedgeo.2006.07.003, 2007.

475 Bezanson, J., Edelman, A., Karpinski, S., and Shah, V. B.: Julia: A Fresh Approach to Numerical Computing, SIAM Rev., 59, 65–98, https://doi.org/10.1137/141000671, 2017.

Bottinelli, N., Jouquet, P., Capowiez, Y., Podwojewski, P., Grimaldi, M., and Peng, X.: Why is the influence of soil macrofauna on soil structure only considered by soil ecologists?, Soil and Tillage Research, 146, 118–124, https://doi.org/10.1016/j.still.2014.01.007, 2015.

480 Briones, M. J. I.: Soil fauna and soil functions: a jigsaw puzzle, Front. Environ. Sci., 2, https://doi.org/10.3389/fenvs.2014.00007, 2014.

Brown, E. T., Colin, F., and Bourlès, D. L.: Quantitative evaluation of soil processes using in situ-produced cosmogenic nuclides, Comptes Rendus Geoscience, 335, 1161–1171, https://doi.org/10.1016/j.crte.2003.10.004, 2003.

Creamer, R. E., Barel, J. M., Bongiorno, G., and Zwetsloot, M. J.: The life of soils: Integrating the who and how of

485 multifunctionality, Soil Biology and Biochemistry, 166, 108561, https://doi.org/10.1016/j.soilbio.2022.108561, 2022.

De Alba, S., Lindstrom, M., Schumacher, T. E., and Malo, D. D.: Soil landscape evolution due to soil redistribution by tillage: a new conceptual model of soil catena evolution in agricultural landscapes, CATENA, 58, 77–100, https://doi.org/10.1016/j.catena.2003.12.004, 2004.

Duller, G. A. T.: Single-grain optical dating of Quaternary sediments: why aliquot size matters in luminescence dating, Boreas,

490 37, 589–612, https://doi.org/10.1111/j.1502-3885.2008.00051.x, 2008.

Furbish, D. J., Roering, J. J., Almond, P., and Doane, T. H.: Soil particle transport and mixing near a hillslope crest: 1. Particle ages and residence times, Journal of Geophysical Research: Earth Surface, 123, 1052–1077, https://doi.org/10.1029/2017JF004315, 2018a.

Furbish, D. J., Roering, J. J., Keen-Zebert, A., Almond, P., Doane, T. H., and Schumer, R.: Soil particle transport and mixing
495   near a hillslope crest: 2. Cosmogenic nuclide and optically stimulated luminescence tracers, Journal of Geophysical Research:
Earth Surface, 123, 1078–1093, https://doi.org/10.1029/2017JF004316, 2018b.

Gabet, E. J.: Gopher bioturbation: field evidence for non-linear hillslope diffusion, Earth Surface Processes and Landforms,
25, 1419–1428, https://doi.org/10.1002/1096-9837(200012)25:13<1419::AID-ESP148>3.0.CO;2-1, 2000.

Gabet, E. J., Reichman, O. J., and Seabloom, E. W.: The effects of bioturbation on soil processes and sediment transport,
500   Annual Review of Earth and Planetary Sciences, 31, 249–273, https://doi.org/10.1146/annurev.earth.31.100901.141314, 2003.

Gliganic, L. A., May, J.-H., and Cohen, T. J.: All mixed up: Using single-grain equivalent dose distributions to identify phases
of   pedogenic   mixing   on   a   dryland   alluvial   fan,   Quaternary   International,   362,   23–33,
https://doi.org/10.1016/j.quaint.2014.07.040, 2015.

Gliganic, L. A., Cohen, T. J., Slack, M., and Feathers, J. K.: Sediment mixing in aeolian sandsheets identified and quantified
505   using   single-grain   optically   stimulated   luminescence,   Quaternary   Geochronology,   32,   53–66,
https://doi.org/10.1016/j.quageo.2015.12.006, 2016.

Gray, H. J., Keen-Zebert, A., Furbish, D. J., Tucker, G. E., and Mahan, S. A.: Depth-dependent soil mixing persists across
climate zones, Proceedings of the National Academy of Sciences, 117, 8750–8756, https://doi.org/10.1073/pnas.1914140117,
2020.

510   Halfen, A. F. and Hasiotis, S. T.: Neoichnological study of the traces and burrowing behaviors of the Western harvester ant
Pogonomyrex Occidentalis (insecta: Hymenoptera: Formicidae): paleopedogenic and paleoecological implications,
PALAIOS, 25, 703–720, https://doi.org/10.2110/palo.2010.p10-005r, 2010.

Hanson, P. R., Mason, J. A., Jacobs, P. M., and Young, A. R.: Evidence for bioturbation of luminescence signals in eolian
sand   on   upland   ridgetops,   southeastern   Minnesota,   USA,   Quaternary   International,   362,   108–115,
515   https://doi.org/10.1016/j.quaint.2014.06.039, 2015.

Heimsath, A. M., Dietrich, W. E., Nishiizumi, K., and Finkel, R. C.: The soil production function and landscape equilibrium,
Nature, 388, 358–361, https://doi.org/10.1038/41056, 1997.

Heimsath, A. M., Chappell, J., Spooner, N. A., and Questiaux, D. G.: Creeping soil, Geology, 30, 111–114, 2002.

Johnson, M. O., Mudd, S. M., Pillans, B., Spooner, N. A., Keith Fifield, L., Kirkby, M. J., and Gloor, M.: Quantifying the rate
520   and depth dependence of bioturbation based on optically-stimulated luminescence (OSL) dates and meteoric 10Be, Earth
Surface Processes and Landforms, 39, 1188–1196, https://doi.org/10.1002/esp.3520, 2014.

Kaste, J. M., Heimsath, A. M., and Bostick, B. C.: Short-term soil mixing quantified with fallout radionuclides, Geology, 35,
243–246, https://doi.org/10.1130/G23355A.1, 2007.

Kraus, D., Brandl, R., Achilles, S., Bendix, J., Grigusova, P., Larsen, A., Pliscoff, P., Übernickel, K., and Farwig, N.:
525   Vegetation and vertebrate abundance as drivers of bioturbation patterns along a climate gradient, PLOS ONE, 17, e0264408,
https://doi.org/10.1371/journal.pone.0264408, 2022.

Kristensen, J. A., Thomsen, K., Murray, A., Buylaert, J.-P., Jain, M., and Breuning-Madsen, H.: Quantification of termite bioturbation in a savannah ecosystem: Application of OSL dating, Quaternary Geochronology, 30, https://doi.org/10.1016/j.quageo.2015.02.026, 2015.

530   Lee, K. E. and Foster, R. C.: Soil fauna and soil structure, Soil Res., 29, 745–775, https://doi.org/10.1071/sr9910745, 1991.

Madsen, A. T., Murray, A. S., Jain, M., Andersen, T. J., and Pejrup, M.: A new method for measuring bioturbation rates in sandy tidal flat sediments based on luminescence dating, Estuarine, Coastal and Shelf Science, 92, 464–471, 2011.

Meng, X., Kooijman, A. M., Temme, A. J. A. M., and Cammeraat, E. L. H.: The current and future role of biota in soil-landscape evolution models, Earth-Science Reviews, 103945, https://doi.org/10.1016/j.earscirev.2022.103945, 2022.

535   Meyer, M. C., Gliganic, L. A., Jain, M., Sohbati, R., and Schmidmair, D.: Lithological controls on light penetration into rock surfaces – Implications for OSL and IRSL surface exposure dating, Radiation Measurements, 120, 298–304, https://doi.org/10.1016/j.radmeas.2018.03.004, 2018.

Michel, E., Néel, M.-C., Capowiez, Y., Sammartino, S., Lafolie, F., Renault, P., and Pelosi, C.: Making Waves: Modeling bioturbation in soils – are we burrowing in the right direction?, Water Research, 216, 118342,

540   https://doi.org/10.1016/j.watres.2022.118342, 2022.

Miedema, R. and Slager, S.: Micromorphological Quantification of Clay Illuviation, Journal of Soil Science, 23, 309–314, https://doi.org/10.1111/j.1365-2389.1972.tb01662.x, 1972.

Minasny, B., Stockmann, U., Hartemink, A. E., and McBratney, A. B.: Measuring and Modelling Soil Depth Functions, in: Digital Soil Morphometrics, edited by: Hartemink, A. E. and Minasny, B., Springer International Publishing, Cham, 225–240,

545   https://doi.org/10.1007/978-3-319-28295-4_14, 2016.

Reimann, T., Román-Sánchez, A., Vanwalleghem, T., and Wallinga, J.: Getting a grip on soil reworking – Single-grain feldspar luminescence as a novel tool to quantify soil reworking rates, Quaternary Geochronology, 42, 1–14, https://doi.org/10.1016/j.quageo.2017.07.002, 2017.

Richards, P.: Aphaenogaster ants as bioturbators: Impacts on soil and slope processes, Earth-Science Reviews, 96, 92–106,

550   https://doi.org/10.1016/j.earscirev.2009.06.004, 2009.

Rink, W. J., Dunbar, J. S., Tschinkel, W. R., Kwapich, C., Repp, A., Stanton, W., and Thulman, D. K.: Subterranean transport and deposition of quartz by ants in sandy sites relevant to age overestimation in optical luminescence dating, Journal of Archaeological Science, 40, 2217–2226, https://doi.org/10.1016/j.jas.2012.11.006, 2013.

Román-Sánchez, A., Reimann, T., Wallinga, J., and Vanwalleghem, T.: Bioturbation and erosion rates along the soil-hillslope

555   conveyor belt, part 1: insights from single-grain feldspar luminescence, Earth Surface Processes and Landforms, 44, 2051–2065, https://doi.org/10.1002/esp.4628, 2019a.

Román-Sánchez, A., Laguna, A., Reimann, T., Giraldez, J., Peña, A., and Vanwalleghem, T.: Bioturbation and erosion rates along the soil-hillslope conveyor belt, part 2: quantification using an analytical solution of the diffusion-advection equation, Earth Surface Processes and Landforms, 44, 2066–2080, https://doi.org/10.1002/esp.4626, 2019b.

560 Ruiz, S., Or, D., and Schymanski, S. J.: Soil Penetration by Earthworms and Plant Roots—Mechanical Energetics of Bioturbation of Compacted Soils, PLOS ONE, 10, e0128914, https://doi.org/10.1371/journal.pone.0128914, 2015.

Sauzet, O., Cammas, C., Gilliot, J., and Montagne, D.: Long-term quantification of the intensity of clay-sized particles transfers due to earthworm bioturbation and eluviation/illuviation in a cultivated Luvisol, Geoderma, 429, https://doi.org/10.1016/j.geoderma.2022.116251, 2023.

565 Schiffers, K., Teal, L. R., Travis, J. M. J., and Solan, M.: An Open Source Simulation Model for Soil and Sediment Bioturbation, PLOS ONE, 6, e28028, https://doi.org/10.1371/journal.pone.0028028, 2011.

Sheather, S. J. and Jones, M. C.: A Reliable Data-Based Bandwidth Selection Method for Kernel Density Estimation, Journal of the Royal Statistical Society. Series B (Methodological), 53, 683–690, 1991.

Stewart, A. D. and Anand, R. R.: Anomalies in insect nest structures at the Garden Well gold deposit: Investigation of mound-
570 forming termites, subterranean termites and ants, Journal of Geochemical Exploration, 140, 77–86, https://doi.org/10.1016/j.gexplo.2014.02.011, 2014.

Stockmann, U., Minasny, B., Pietsch, T. J., and McBratney, A. B.: Quantifying processes of pedogenesis using optically stimulated luminescence, European Journal of Soil Science, 64, 145–160, https://doi.org/10.1111/ejss.12012, 2013.

von Suchodoletz, H., Kühn, P., Wiedner, K., and Reimann, T.: Deciphering timing and rates of Central German
575 Chernozem/Phaeozem formation through high resolution single-grain luminescence dating, Scientific Reports, 13, 4769, https://doi.org/10.1038/s41598-023-32005-9, 2023.

Taylor, A. R., Lenoir, L., Vegerfors, B., and Persson, T.: Ant and Earthworm Bioturbation in Cold-Temperate Ecosystems, Ecosystems, 22, 981–994, https://doi.org/10.1007/s10021-018-0317-2, 2019.

Temme, A. J. A. M. and Vanwalleghem, T.: LORICA – A new model for linking landscape and soil profile evolution:
580 development and sensitivity analysis, Computers & Geosciences, 90, 131–143, https://doi.org/10.1016/j.cageo.2015.08.004, 2016.

Tyler, A. N., Carter, S., Davidson, D. A., Long, D. J., and Tipping, R.: The extent and significance of bioturbation on 137Cs distributions in upland soils, CATENA, 43, 81–99, https://doi.org/10.1016/S0341-8162(00)00127-2, 2001.

Van der Meij, W. M. and Temme, A. J. A. M.: ChronoLorica v1.0, Zenodo [code], https://doi.org/10.5281/zenodo.7875033,
585 2022.

Van der Meij, W. M., Reimann, T., Vornehm, V. K., Temme, A. J. A. M., Wallinga, J., van Beek, R., and Sommer, M.: Reconstructing rates and patterns of colluvial soil redistribution in agrarian (hummocky) landscapes, Earth Surface Processes and Landforms, 44, 2408–2422, https://doi.org/10.1002/esp.4671, 2019.

Van der Meij, W. M., Temme, A. J., Wallinga, J., and Sommer, M.: Modeling soil and landscape evolution–the effect of
590 rainfall and land-use change on soil and landscape patterns, Soil, 6, 337–358, https://doi.org/10.5194/soil-6-337-2020, 2020.

Van der Meij, W. M., Temme, A. J. A. M., Binnie, S. A., and Reimann, T.: ChronoLorica: introduction of a soil–landscape evolution model combined with geochronometers, Geochronology, 5, 241–261, https://doi.org/10.5194/gchron-5-241-2023, 2023.

Wilkinson, M. T., Richards, P. J., and Humphreys, G. S.: Breaking ground: Pedological, geological, and ecological
595 implications of soil bioturbation, Earth-Science Reviews, 97, 257–272, https://doi.org/10.1016/j.earscirev.2009.09.005, 2009.

Wintle, A. G. and Murray, A. S.: A review of quartz optically stimulated luminescence characteristics and their relevance in
single-aliquot regeneration dating protocols, Radiation measurements, 41, 369–391, 2006.

Yates, L. A., Aandahl, Z., Brook, B. W., Jacobs, Z., Li, B., David, B., and Roberts, R. G.: A new OSL dose model to account
for post-depositional mixing of sediments, Quaternary Geochronology, 101502,
600 https://doi.org/10.1016/j.quageo.2024.101502, 2024.